RSC Advances

PAPER

View Article Online
View Journal | View Issue

Cite this: *RSC Adv.*, 2026, **16**, 5887

Effect of *para*-aryl-substituted *N*-phenyl groups on the photophysical properties of highly fluorescent dibenzo[*c*,*g*]carbazole-based chromophores

Minwoo Kong,[ac] Ji Hye Lee,[b] Heekyung Park,[c] Hyonseok Hwang,[b] Junseong Lee,[d] Jun Hui Park,[c] Myung Hwan Park *[a] and Houng Kang *[a]

Received 27th November 2025
Accepted 20th January 2026

DOI: 10.1039/d5ra09166g

rsc.li/rsc-advances

Dibenzo[*c*,*g*]carbazole (DBC) derivatives are an emerging class of fused-ring carbazole chromophores that exhibit promising optoelectronic properties. However, challenges with their synthesis mean that their photophysical properties remain poorly understood. In this study, we successfully synthesized a series of DBC-based chromophores bearing *para*-aryl-substituted *N*-phenyl groups (Ar = phenyl, naphthyl, anthracenyl, pyrenyl, and carbazolyl). We then elucidated the structure–property relationships that govern their photophysical behavior. The DBC core scaffold was established through the Cu(II)-catalyzed oxidative tandem coupling and cyclization of 2-naphthylamine, followed by Suzuki or Buchwald–Hartwig coupling to introduce extended aromatic substituents. All compounds exhibited strong absorption in the 305–367 nm range and intense emission with high photoluminescence quantum yields (Φ_{PL} = 74–97% in solution and 67–74% in film). Theoretical calculations revealed that a moderately twisted geometry between the DBC moiety and *para*-aryl-substituted *N*-phenyl unit allowed for locally excited π–π^* transitions with partial intramolecular charge transfer, resulting in red-shifted emission. The impressive emission efficiencies and thermal stabilities of these DBC-based chromophores make them promising candidates for high-performance optoelectronic materials.

Introduction

Fused-ring carbazole derivatives have received significant attention for use in optoelectronic applications such as organic light-emitting diodes (OLEDs),[1–4] perovskite solar cells (PSCs),[5,6] sensors,[7,8] and electrochromic devices.[9,10] As electron-rich building blocks, carbazole derivatives exhibit strong electron-donating and hole-transporting properties, along with high thermal and electrochemical stabilities.[11–13] The structural and electronic properties of fused-ring carbazole derivatives can be easily adjusted by introducing different substituents, which has broadened their application scope.[14] Research on the functionalization of carbazole units has primarily focused on carbazole-based derivatives, including indolocarbazole (**I**), indenocarbazole (**II**), benzofurocarbazole (**III**), and diindolocarbazole (**IV**) (Fig. 1).[15] However, dibenzo[*c*,*g*]carbazoles (DBCs, **V**), which are highly efficient chromophores and emitters, have been less studied owing to challenges associated with their synthesis.[16–19]

The core DBC backbone was first obtained in 2001, when Kočovský and co-workers reported that DBCs could be formed as byproducts during the oxidative coupling of naphthols.[20] However, few synthetic strategies have been developed since. Notably, Cho and colleagues demonstrated that DBCs can be prepared from 2,2′-diamino-1,1′-biaryls in the presence of a strong acid, such as HCl.[21] This provides an alternative route that Kočovský's group had previously considered to be inaccessible.[20] In another study, Patureau and colleagues developed

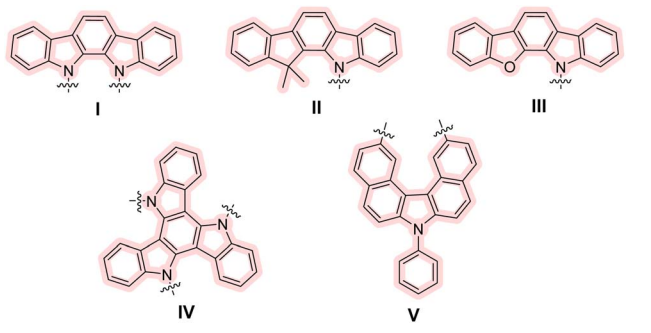

Fig. 1 Functionalized fused-ring carbazole derivatives (**I**–**IV**) and previously developed dibenzo[*c*,*g*]carbazoles (**V**).

[a]*Department of Chemistry Education, Chungbuk National University, Cheongju, Chungbuk 28644, Republic of Korea. E-mail: mhpark98@chungbuk.ac.kr; hkang@chungbuk.ac.kr*

[b]*Department of Chemistry and Institute for Molecular Science and Fusion Technology, Kangwon National University, Chuncheon, Gangwon 24341, Republic of Korea*

[c]*Department of Chemistry, Chungbuk National University, Cheongju, Chungbuk 28644, Republic of Korea*

[d]*Department of Chemistry, Chonnam National University, Gwangju 61186, Republic of Korea*

one of the few synthetically useful routes to DBCs.[22] However, its reliance on stoichiometric Ag_2O greatly limits its practicality and scalability. Recently, we developed a Cu(II)-catalyzed oxidative tandem coupling and cyclization method for 2-aminonaphthalenes, which allows for the catalytic synthesis of DBC derivatives under mild conditions.[23] The DBC derivatives with substituents on the *N*-phenyl groups or naphthalene moieties exhibited photoluminescence quantum yields (PLQYs) of up to 100%, demonstrating their potential as promising optoelectronic materials.

Owing to the synthetic challenges associated with DBCs, their photophysical properties remain poorly understood. Therefore, in this study, we built upon the aforementioned synthetic advances to design and synthesize a series of DBC-based compounds with different *para*-aryl-substituents, including phenyl, naphthyl, anthracenyl, pyrenyl, and carbazolyl groups, on the *N*-phenyl units, and analyzed their photophysical properties in detail. We also performed density functional theory (DFT) calculations to support the experimental findings. The results establish DBC derivatives as stable and tunable chromophores and provide design guidelines for their application in high-efficiency organic emitters and related photonic materials.

Experimental section

General considerations

All manipulations were conducted under an inert N_2 atmosphere using standard Schlenk techniques and glove box methods. All solvents were dried by passing them through an activated alumina column and stored over activated molecular sieves (5 Å). All solvents were of spectrophotometric grade and used as received. All commercial reagents were purchased from TCI, Sigma-Aldrich, or Alfa Aesar and used without further purification. All deuterated solvents ($CDCl_3$) were obtained from Cambridge Isotope Laboratories and used after drying over activated molecular sieves (5 Å). ^{1}H (500 MHz) and ^{13}C NMR (125 MHz) spectra were recorded at ambient temperature using a Bruker Avance 500 MHz NMR spectrometer. All chemical shifts are reported in parts per million (ppm, δ) and referenced against the chemical shift of residual $CDCl_3$ (δ = 7.26 for ^{1}H NMR; δ = 77.16 for ^{13}C NMR). High-resolution mass spectrometry (HRMS) was performed using a Waters Xevo G2-XS QTof instrument. Infrared (IR) spectra were collected using IROS 05 and Bruker ALPHA Fourier-transform infrared (FT-IR) spectrometers. The results are presented in reciprocal centimeters (cm^{-1}), and only selected absorbance peaks are reported.

General synthesis of 7-(Ar)-7*H*-dibenzo[*c*,*g*]carbazoles (DBC-Ph, DBC-Nap, DBC-Ant, and DBC-Pyr)

A microvial was charged with 7-(4-bromophenyl)-7*H*-dibenzo[*c*,*g*]carbazole (1.0 equiv.), phenylboronic acid (1.3 equiv.), tetrakis(triphenylphosphine)palladium(0) ($Pd(PPh_3)_4$; 0.1 equiv.), and either Na_2CO_3 (8.0 equiv.) or K_2CO_3 (8.0 equiv.). Subsequently, either a mixed solvent (toluene (2.0 M), distilled water (0.25 M), and ethanol (1.0 M)) or 1,4-dioxane (0.25 M) was added. The mixture was then refluxed for 16 h, allowed to cool to room temperature, and extracted using ethyl acetate (EtOAc; 5 mL × 3). The combined organic layers were then washed with brine, dried over $MgSO_4$, and filtered. Finally, the solvents were removed under reduced pressure, and the products were purified using column chromatography.

Synthesis of 7-([1,1′-biphenyl]-4-yl)-7*H*-dibenzo[*c*,*g*]carbazole (DBC-Ph)

The reaction was conducted using 7-(4-bromophenyl)-7*H*-dibenzo[*c*,*g*]carbazole (200 mg, 0.47 mmol), phenylboronic acid (75.0 mg, 0.62 mmol), $Pd(PPh_3)_4$ (54.7 mg, 0.047 mmol), and Na_2CO_3 (402 mg, 3.76 mmol) in a mixture of toluene (1.89 mL), distilled water (1.89 mL), and ethanol (0.47 mL). The desired product, **DBC-Ph**, was obtained as a white solid (119.7 mg, 60% yield). m.p.: 298–299 °C; FT-IR (neat, cm^{-1}): 3059, 3029, 1732, 1594, 1519, 1486, 793, 738, 690. ^{1}H NMR ($CDCl_3$, 500 MHz): δ 9.28 (2H, d, J = 8.4 Hz, Ar), 8.06 (2H, d, J = 7.8 Hz, Ar), 7.88 (2H, d, J = 8.2 Hz, Ar), 7.86 (2H, d, J = 8.7 Hz, Ar), 7.75–7.70 (4H, m, Ar), 7.65 (4H, t, J = 9.7 Hz, Ar), 7.57–7.51 (4H, m, Ar), 7.45 (1H, t, J = 7.5 Hz, Ar). ^{13}C{^{1}H} NMR ($CDCl_3$, 125 MHz): δ 141.49, 140.27, 138.16, 136.23, 130.38, 129.29, 129.25, 129.18, 128.76, 128.66, 128.00, 127.38, 126.96, 125.64, 125.47, 123.63, 117.87, 111.99. HRMS (SI, m/z), found: $[M + H]^+$ 420.1738; molecular formula $C_{32}H_{22}N$ requires $[M + H]^+$ 420.1752.

Synthesis of 7-(4-(naphthalen-1-yl)phenyl)-7*H*-dibenzo[*c*,*g*]carbazole (DBC-Nap)

The reaction was conducted using 7-(4-bromophenyl)-7*H*-dibenzo[*c*,*g*]carbazole (150 mg, 0.36 mmol), 2-naphthylboronic acid (79.4 mg, 0.46 mmol), $Pd(PPh_3)_4$ (41.0 mg, 0.036 mmol), and Na_2CO_3 (301 mg, 2.84 mmol) in a mixture of toluene (1.42 mL), distilled water (1.42 mL), and ethanol (0.36 mL). The desired product, **DBC-Nap**, was obtained as a white solid (110.4 mg, 66% yield). m.p.: 213–215 °C; FT-IR (neat, cm^{-1}): 3057, 3045, 1610, 1593, 1505, 796, 737, 764. ^{1}H NMR ($CDCl_3$, 500 MHz): δ 9.31 (2H, d, J = 8.6 Hz, Ar), 8.11–8.06 (3H, m, Ar), 8.00–7.94 (2H, m, Ar), 7.91 (2H, d, J = 8.9 Hz, Ar), 7.80 (2H, d, J = 8.4 Hz, Ar), 7.76–7.70 (6H, m, Ar), 7.64–7.54 (6H, m, Ar). ^{13}C{^{1}H} NMR ($CDCl_3$, 125 MHz): δ 141.09, 139.28, 138.18, 136.22, 134.08, 131.75, 131.65, 130.41, 129.31, 129.28, 128.65, 128.36, 128.17, 127.35, 126.99, 126.56, 126.18, 125.91, 125.67, 125.62, 125.49, 123.66, 117.91, 112.05. HRMS (ESI, m/z), found: $[M + H]^+$ 470.1917; molecular formula $C_{36}H_{24}N$ requires $[M + H]^+$ 470.1909.

Synthesis of 7-(4-anthracen-9-yl)phenyl)-7*H*-dibenzo[*c*,*g*]carbazole (DBC-Ant)

The reaction was conducted using 7-(4-bromophenyl)-7*H*-dibenzo[*c*,*g*]carbazole (50 mg, 0.12 mmol), 9-anthraceneboronic acid (34.2 mg, 0.15 mmol), $Pd(PPh_3)_4$ (14.0 mg, 0.012 mmol), and K_2CO_3 (130 mg, 0.95 mmol) in 1,4-dioxane (0.47 mL). The desired product, **DBC-Ant**, was obtained as a brown solid (54.6 mg, 89% yield). m.p.: 251–253 °C; FT-IR (neat, cm^{-1}): 3080, 3046, 1666, 1594, 1514, 933, 800, 723. ^{1}H NMR ($CDCl_3$, 500

MHz): δ 9.33 (2H, d, J = 8.6 Hz, Ar), 8.59 (1H, s, Ar), 8.12 (4H, t, J = 8.1 Hz, Ar), 7.95 (2H, d, J = 8.9 Hz, Ar), 7.86 (2H, t, J = 8.7 Hz, Ar), 7.82 (4H, d, J = 9.0 Hz, Ar), 7.78–7.72 (4H, m, Ar), 7.61–7.47 (6H, m, Ar). $^{13}C\{^1H\}$ NMR ($CDCl_3$, 125 MHz): δ 139.22, 138.16, 136.41, 135.81, 133.05, 131.57, 130.45, 130.40, 129.34, 129.30, 128.71, 128.25, 127.31, 127.04, 126.64, 125.96, 125.70, 125.51, 125.43, 123.69, 117.99, 112.05. HRMS (ESI, m/z), found: $[M + H]^+$ 520.2073; molecular formula $C_{40}H_{26}N$ requires $[M + H]^+$ 520.2065.

Synthesis of 7-(4-(pyren-1-yl)phenyl)-7*H*-dibenzo[*c*,*g*]carbazole (DBC-Pyr)

The reaction was conducted using 7-(4-bromophenyl)-7*H*-dibenzo[*c*,*g*]carbazole (50 mg, 0.12 mmol), 2-pyrene-1-boronic acid (38.0 mg, 0.15 mmol), $Pd(PPh_3)_4$ (14.0 mg, 0.012 mmol), and Na_2CO_3 (100 mg, 0.95 mmol) in a mixture of toluene (0.47 mL), distilled water (0.47 mL), and ethanol (0.12 mL). The desired product, **DBC-Pyr**, was obtained as a pale yellow solid (30.9 mg, 48% yield). m.p.: 286–288 °C; FT-IR (neat, cm^{-1}): 3049, 3031, 1593, 1519, 1455, 842, 792, 744. ^1H NMR ($CDCl_3$, 500 MHz): δ 9.31 (2H, d, J = 8.6 Hz, Ar), 8.36 (1H, d, J = 9.2 Hz, Ar), 8.32 (1H, d, J = 7.8 Hz, Ar), 8.24 (2H, t, J = 7.5 Hz, Ar), 8.17–8.05 (7H, m, Ar), 7.93 (4H, dd, J_1 = 8.4 Hz, J_2 = 4.0 Hz, Ar), 7.78 (4H, dd, J_1 = 8.4 Hz, J_2 = 4.4 Hz, Ar), 7.74 (2H, t, J = 7.5 Hz, Ar), 7.57 (2H, t, J = 7.4 Hz, Ar). $^{13}C\{^1H\}$ NMR ($CDCl_3$, 125 MHz): δ 141.53, 138.20, 136.61, 136.24, 132.26, 131.68, 131.13, 130.44, 129.33, 129.29, 128.71, 128.26, 128.09, 127.92, 127.78, 127.57, 127.03, 126.34, 125.69, 125.56, 125.51, 125.24, 125.09, 124.96, 123.68, 117.96, 112.07. HRMS (SI, m/z), found: $[M + H]^+$ 544.2061; molecular formula $C_{42}H_{26}N$ requires $[M + H]^+$ 544.2065.

Synthesis of 7-(4-(9*H*-carbazol-9-yl)phenyl)-7*H*-dibenzo[*c*,*g*]carbazole (DBC-Cbz)

7-(4-Bromophenyl)-7*H*-dibenzo[*c*,*g*]carbazole (50 mg, 0.12 mmol), carbazole (24 mg, 0.14 mmol), palladium(II) acetate ($Pd(OAc)_2$; 1.3 mg, 0.006 mmol), (4-(*N*,*N*-dimethylamino)phenyl) di-*tert*-butyl phosphine (APhos; 3.2 mg, 0.012 mmol), and K_3PO_4 (75.0 mg, 0.36 mmol) were added to a microvial along with 1,4-dioxane (2.37 mL). The mixture was refluxed for 16 h, allowed to cool to room temperature, and then extracted with EtOAc (5 mL × 3). Subsequently, the combined organic layers were washed with brine, dried over $MgSO_4$, and filtered. The solvent was then removed under reduced pressure, and the product was purified using column chromatography. The desired product, **DBC-Cbz**, was obtained as a white solid (53.4 mg, 89% yield). m.p.: 282–283 °C; FT-IR (neat, cm^{-1}): 3042, 3013, 1594, 1514, 1447, 858, 794, 718. ^1H NMR ($CDCl_3$, 500 MHz): δ 9.30 (2H, d, J = 8.5 Hz, Ar), 8.22 (2H, d, J = 7.8 Hz, Ar), 8.09 (2H, d, J = 8.1 Hz, Ar), 7.92 (2H, d, J = 8.9 Hz, Ar), 7.89 (2H, d, J = 8.7 Hz, Ar), 7.83 (2H, d, J = 8.6 Hz, Ar), 7.77–7.70 (4H, m, Ar), 7.63 (2H, d, J = 8.3 Hz, Ar), 7.57 (2H, t, J = 7.6 Hz, Ar), 7.52 (2H, t, J = 7.7 Hz, Ar), 7.38 (2H, t, J = 7.4 Hz, Ar). $^{13}C\{^1H\}$ NMR ($CDCl_3$, 125 MHz): δ 140.81, 138.05, 137.90, 135.91, 130.46, 129.76, 129.34, 129.24, 128.49, 127.16, 126.35, 125.77, 125.50, 123.84, 123.79, 120.66, 120.58, 118.06, 111.78, 109.90. HRMS (SI, m/z), found: $[M + H]^+$ 509.2013; molecular formula $C_{38}H_{25}N_2$ requires $[M + H]^+$ 509.2018.

X-ray crystallography

For X-ray analysis, single crystals of **DBC-Nap** were obtained by the slow evaporation of a solution of **DBC-Nap** in a dichloromethane/hexane mixture at room temperature. A single crystal was coated with Paratone oil and mounted on a glass capillary. Crystallographic measurements were conducted using a Bruker APEX II diffractometer with a charge-coupled device (CCD) detector and graphite-monochromated Mo Kα radiation (λ = 0.71073 Å) at a temperature of 150 K. The structure was determined using direct methods, and all non-hydrogen atoms underwent anisotropic refinement through a full-matrix least-squares method on F^2 in SHELXTL/PC. The X-ray crystallographic data for **DBC-Nap** were obtained in CIF format (CCDC: 2499642). The hydrogen atoms were positioned according to their geometrically calculated locations and refined using the riding model based on the corresponding carbon atoms, with isotropic thermal parameters applied. Detailed crystallographic data are provided in Tables S1 and S2.

Optical and thermal measurements

UV-vis absorption and photoluminescence (PL) spectra were acquired using Cary 8454 (Agilent) and FluoroMax Plus (HORIBA) spectrophotometers, respectively, in oxygen-free solutions (10 μM in toluene, tetrahydrofuran (THF), or MeCN) with a 1 cm quartz cuvette. PL spectra were also recorded in the film state on quartz plates at room temperature. The absolute PLQYs of all compounds were measured using the FluoroMax Plus spectrophotometer (HORIBA) equipped with a 3.2-inch Fluorolog-QM integrating sphere (HORIBA). Cyclic voltammetry (CV) was conducted using a 760E potentiostat (CH Instruments) in acetonitrile (MeCN; 1 mM) containing 50 or 100 mM tetrabutylammonium hexafluorophosphate ($TBAPF_6$) as a supporting electrolyte. The measurements were carried out in three-electrode cells inside a Faraday cage. The working, counter, and reference electrodes were a Pt disk (diameter: 3 mm), Pt wire, and Ag/Ag^+ (10 mM $AgNO_3$ in MeCN), respectively. All measurements were conducted after more than 30 min of Ar bubbling at ambient temperature to remove O_2 from the electrolyte solution. The oxidation potentials were recorded at a scan rate of 100 mV s^{-1} and are reported relative to a ferrocene/ferrocenium (Fc/Fc^+) redox couple. Thermogravimetric analysis (TGA) was performed from 50 to 800 °C (heating rate: 10 °C min^{-1}) under a N_2 atmosphere using a HITACHI NEXTA STA200 instrument.

Theoretical calculations

The optimized structures of **DBC-Ph**, **DBC-Nap**, **DBC-Ant**, **DBC-Pyr**, and **DBC-Cbz** in their ground (S_0) and first excited (S_1) states were determined using DFT with the B3LYP functional.[24] The 6-31+G(d,p) basis set was used for all atoms.[25] The electronic transition energies, with consideration to electron correlation, were obtained from time-dependent density functional theory (TD-DFT) calculations using the hybrid B3LYP functional.[26] All calculations were performed using Gaussian 16.[27] GaussSum 3.0 was used to calculate the percentage

contributions of different groups within a molecule to each molecular orbital.[28]

Results and discussion

Synthesis and characterization

The synthetic routes to the DBC-based compounds **DBC-Ph**, **DBC-Nap**, **DBC-Ant**, **DBC-Pyr**, and **DBC-Cbz** are illustrated in Scheme 1. The core DBC scaffold was obtained in a single step through the tandem oxidative coupling and cyclization of 2-naphthylamine (**1**) under Cu(II)-catalyzed conditions.[23] The resulting DBC intermediate (**2**) was then subjected to Suzuki coupling with various arylboronic acids (**3**), allowing for the introduction of extended aromatic substituents (**DBC-Ph**, **DBC-Nap**, **DBC-Ant**, and **DBC-Pyr**). The reactions proceeded smoothly under the modified conditions, resulting in the desired derivatives in moderate to good yield (48–89%). In the case of **DBC-Cbz**, the desired product was obtained *via* the Pd-catalyzed C–N cross-coupling of (**2**) with carbazole (**4**), resulting in the corresponding derivative in good yield (88%).

The solid-state structure of **DBC-Nap** was confirmed through single-crystal X-ray crystallography (Fig. 2, Tables S1 and S2). The dihedral angle (C1–N1–C21–C26) between the DBC moiety and *para*-substituted phenyl unit was measured as 53.3°, indicating a moderately twisted connection.

Photophysical, electrochemical, and thermal properties

The photophysical properties of DBC-based compounds **DBC-Ph**, **DBC-Nap**, **DBC-Ant**, **DBC-Pyr**, and **DBC-Cbz**, which contain *para*-aryl-substituents on the *N*-phenyl group, were investigated using UV-vis absorption and PL spectroscopy in oxygen-free diluted toluene (10 μM) at 298 K (Table 1, Fig. 3a and b). The absorption spectra all exhibited similar characteristic peaks (Fig. 3a). The high-energy band at 305–307 nm and low-energy band at 350 nm correspond to local π–π* and *n*–π* transitions centered on the DBC moiety, respectively, whereas the band at 367 nm corresponds to partial intramolecular charge

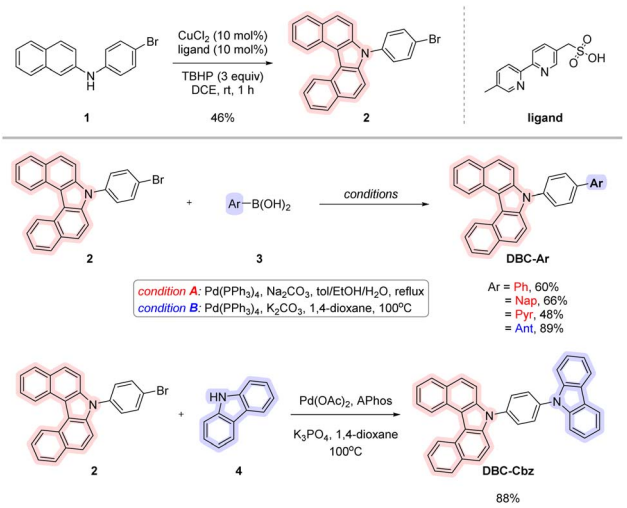

Scheme 1 Synthetic procedure for synthesizing DBC-based compounds DBC-Ph, DBC-Nap, DBC-Ant, DBC-Pyr, and DBC-Cbz.

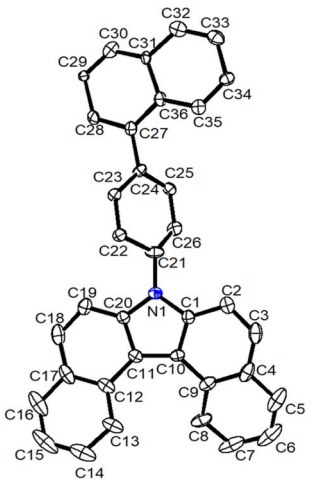

Fig. 2 Structure of DBC-Nap (50% thermal ellipsoids), as determined by X-ray crystallography. H atoms are omitted for clarity.

transfer (ICT) between the DBC moiety and *para*-substituted *N*-phenyl unit, similar to that observed for other DBC derivatives.[17,23] Two further absorption peaks were observed at 334 and 387 nm for **DBC-Ant**, whereas weak shoulder peaks appeared at approximately 336 and 380 nm for **DBC-Pyr.** These features are attributed to the π–π* transitions of the *para*-substituted groups (anthracene in **DBC-Ant** and pyrene in **DBC-Pyr**).[29,30]

The electrochemical properties of the DBC derivatives were investigated by CV in deoxygenated MeCN (1 mM) and thin film (Table 1, Fig. S6 and S7). All compounds underwent irreversible oxidation in both solution and thin film. In solution, the highest occupied molecular orbital (HOMO) energies of **DBC-Cbz**, **DBC-Nap**, **DBC-Ant**, and **DBC-Pyr**, as determined from the oxidation onset potentials, were almost identical at −5.47 eV, whereas that of **DBC-Ph** was −5.23 eV. The lowest unoccupied molecular orbital (LUMO) energies, as calculated from the HOMO energies and optical bandgaps (E_g), ranged from −1.93 to −2.35 eV for all compounds, with slight variations depending on the *para*-aryl-substituent of the *N*-phenyl group (Table 1). The thermal stabilities of the DBC-based compounds were examined using TGA (Table 1 and Fig. 4). The onset of thermal degradation (5% weight loss temperature, T_{d5}) occurred between 330 and 438 °C for all compounds, indicating high thermal stability.

The PL emission spectra of **DBC-Ph**, **DBC-Nap**, and **DBC-Cbz** exhibited nearly identical broad dual emission peaks within the range of 374–393 nm (Fig. 3b). These peaks are attributed to the π–π* transition associated with the DBC moiety, combined with partial charge transfer (CT) from the DBC moiety to the *N*-phenyl unit.[23] Additionally, low-energy shoulders and long tails associated with the ICT appeared at approximately 420 nm and beyond 470 nm, respectively. The emission wavelengths of these compounds did not deviate, regardless of the *para*-substituent (phenyl, naphthyl, or carbazolyl) on the *N*-phenyl group. However, the emission spectra of **DBC-Ant** and **DBC-Pyr** differed significantly, with broad, structureless bands centered at 406 and 395 nm, respectively. These bands correspond to the π–π*

Table 1 Photophysical, electrochemical, and thermal data of DBC-based compounds

Compound	λ_{abs}[a] [nm] ($\varepsilon \times 10^{-3}$ M^{-1} cm^{-1})	λ_{em} [nm]			Φ_{PL}[c] [%]			HOMO[d]/LUMO[e] [eV]	E_g[f] [eV]	T_{d5}[g] [°C]
		Toluene[a]	THF[a]	Film[b]	Toluene[a]	THF[a]	Film[b]			
DBC-Ph	307 (11.3), 350 (5.4), 367 (7.1)	374, 393	374, 392	412, 418	92	96	70	−5.23/−1.93	3.30	358
DBC-Nap	307 (25.8), 350 (13.5), 367 (18.2)	375, 393	374, 392	413	84	78	74	−5.47/−2.18	3.29	374
DBC-Ant	306 (17.0), 334 (9.0), 350 (20.0), 367 (29.5), 387 (9.5)	406, 422	403, 422	421, 424	80	81	67	−5.47/−2.35	3.12	383
DBC-Pyr	305 (14.6), 350 (23.9), 367 (20.6)	395	395	463	94	83	69	−5.47/−2.21	3.26	438
DBC-Cbz	307 (19.0), 350 (10.3), 367 (13.9)	375, 393	374, 391	407, 414	74	97	70	−5.47/−2.18	3.29	330

[a] In oxygen-free toluene (1.0×10^{-5} M) at 298 K. [b] In a spin-coated neat film of compound. [c] Absolute PLQY. [d] Calculated from the oxidation onset potential in MeCN *vs.* a ferrocene/ferrocenium (Fc/Fc^+) couple. [e] Estimated from the HOMO and band-gap (E_g) energies. [f] Estimated from the absorption edge in MeCN solution (1.0×10^{-5}M). [g] Estimated from the 5% weight loss temperature measured by TGA under N_2.

transition associated with the DBC moiety, as well as partial ICT behavior between the DBC moiety and *para*-aryl substituted *N*-phenyl group (see the theoretical results). These bands were red-shifted in comparison to those of **DBC-Ph**, **DBC-Nap**, and **DBC-Cbz**. Additional weak emission shoulders appeared at approximately 415 nm for **DBC-Pyr** and 422 nm for **DBC-Ant**, corresponding to the π–π* transitions associated with the pyrenyl and anthracenyl groups, respectively.[17,23] In more polar solvents, such as THF and MeCN, no variation in emission bands was observed, indicating weak CT characteristics (Table 1 and Fig. S8). The emission profiles of all DBC-based compounds in their film state aligned well with the trends observed in solution (Table 1 and Fig. S9).

The absolute PLQYs (Φ_{PL}) of the DBC-based compounds were measured in both oxygen-free solutions and in films (Table 1). All compounds demonstrated high emission intensities in solution, with Φ_{PL} values ranging from 74% to 94% in toluene and from 78% to 97% in THF. However, the Φ_{PL} values decreased significantly to below 42% in MeCN, which has higher polarity (Table S3 and S4). In a film state, the Φ_{PL} values of DBC-based compounds (67–74%) were slightly decreased compared to those in solutions (toluene and THF), implying that aggregation-caused quenching (ACQ) occurred in the rigid state. Overall, the high PLQYs of the DBC-based compounds support their potential as effective chromophores in optoelectronic materials.

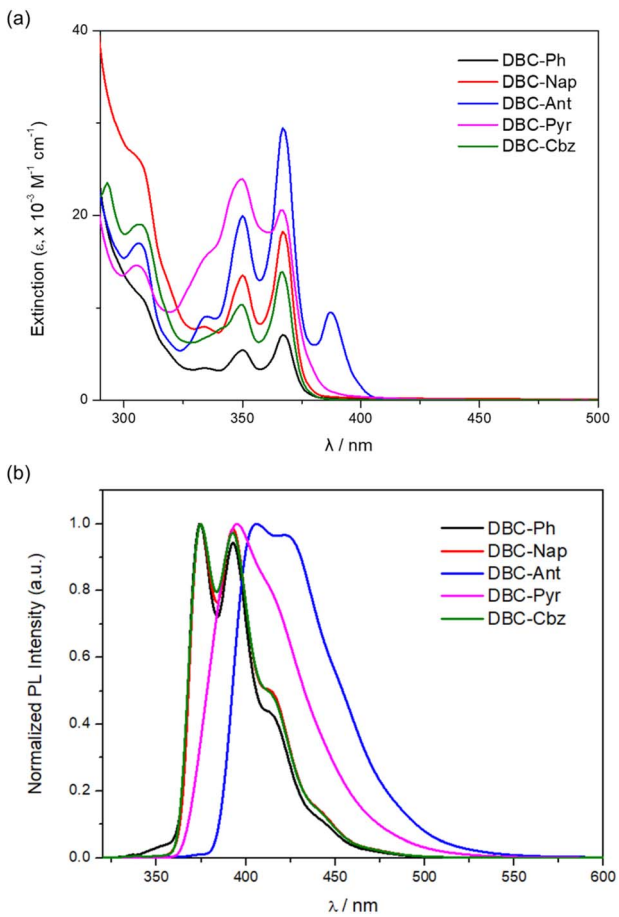

Fig. 3 (a) UV-vis absorption and (b) PL spectra of DBC-based compounds (**DBC-Ph**, **DBC-Nap**, **DBC-Cbz**, **DBC-Ant**, and **DBC-Pyr**) (λ_{ex} = 305–334 nm) in toluene (1.0×10^{-5} M).

Theoretical calculations

To elucidate the frontier molecular orbital distributions and electronic transitions of the DBC derivatives in their ground (S_0) and first excited (S_1) states, we conducted TD-DFT calculations

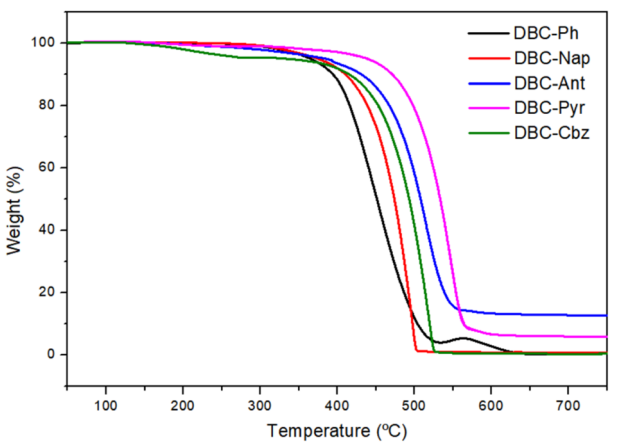

Fig. 4 (a) TGA curves of DBC-based compounds (**DBC-Ph**, **DBC-Nap**, **DBC-Cbz**, **DBC-Ant**, and **DBC-Pyr**).

Table 2 Dihedral angles (°) between the DBC moieties, *N*-phenyl units, and *para*-substituted aryl groups in the optimized S_0 state structures of DBC-based compounds

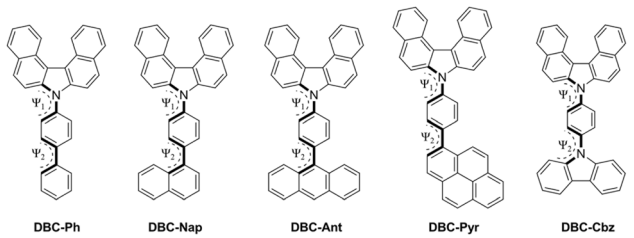

Compound					
dihedral angle [°]	**DBC-Ph**	**DBC-Nap**	**DBC-Ant**	**DBC-Pyr**	**DBC-Cbz**
Ψ_1	64.7	65.0	63.0	64.7	64.1
Ψ_2	39.0	59.3	79.8	79.8	58.6

using the B3LYP functional and 6-31 + G(d,p) basis set (Table 2, S5–S14, Fig. 5 and S10–S15). To account for solvent (toluene) effects, we employed the integral equation formalism polarizable continuum model (IEFPCM).[31] The optimized S_0 structures of the DBC-based compounds exhibited a dihedral angle of 63°–65° between the DBC moiety and *N*-phenyl group, which is comparable to the value of 53.3° observed in the X-ray crystallography-derived structure of **DBC-Nap**. The dihedral angle between the *N*-phenyl unit and *para*-aryl-substituent was significantly larger for **DBC-Ant** and **DBC-Pyr** (approximately 80°; Table 2) than for **DBC-Ph**, **DBC-Nap**, and **DBC-Cbz** (39°–59°; Table 2). The near-perpendicular arrangements of **DBC-Ant** and **DBC-Pyr** resulted in clear spatial separation of the HOMO and LUMO. Specifically, these orbitals were localized on the DBC moiety and *para*-substituted *N*-phenyl unit, respectively, resembling a typical donor–acceptor arrangement. By contrast, **DBC-Ph**, **DBC-Nap**, and **DBC-Cbz** exhibited a moderately twisted geometry between the DBC and *N*-phenyl groups. This configuration caused the HOMO to be located primarily on the DBC moiety, whereas the LUMO was distributed across the *para*-substituted *N*-phenyl group and partially extended into the DBC moiety (Fig. 5).

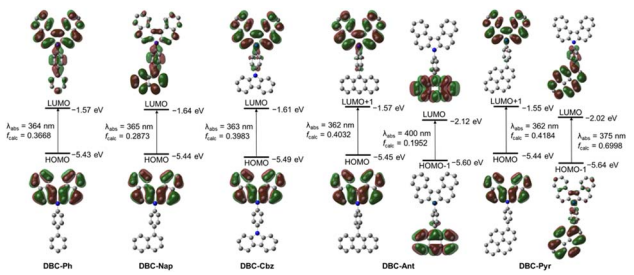

Fig. 5 Frontier molecular orbitals of DBC-based compounds (**DBC-Ph**, **DBC-Nap**, **DBC-Cbz**, **DBC-Ant**, and **DBC-Pyr**) in their S_0 states with relative energies obtained *via* DFT (isovalue = 0.02). The corresponding transition energy (in nm) was calculated using the TD-B3LYP method with the 6-31 + G(d,p) basis set.

The calculation results for the S_0 states of **DBC-Ph**, **DBC-Nap**, and **DBC-Cbz** indicated that the primary low-energy absorption band was mainly associated with the HOMO–LUMO transition (Fig. 5). For these compounds, the HOMO was localized entirely within the DBC group (100%), whereas the LUMO was distributed across both the DBC and *para*-substituted *N*-phenyl moieties. This indicates that the primary low-energy absorption process arose from a significant locally excited (LE) π–π* transition centered on the DBC group, along with partial CT from the DBC moiety to the *para*-substituted *N*-phenyl unit. Interestingly, the major absorption process in **DBC-Ant** and **DBC-Pyr** resulted from two separate LE π–π* transitions: one occurring within the DBC moiety (high energy) and the other in the *para*-substituted *N*-phenyl unit (low energy). Despite the spatial separation of the HOMO and LUMO in **DBC-Ant** and **DBC-Pyr**, no significant ICT-based HOMO–LUMO transition was observed. Furthermore, in the S_1 state, the emission processes of all DBC-based compounds closely resembled those of the absorption processes (Fig. S14). These findings align with the absence of solvatochromic effects observed in the experimental results.

Conclusions

In summary, we developed an efficient synthetic route for DBC-based chromophores with various *para*-aryl-substituted *N*-phenyl groups, and systematically studied their photophysical, electrochemical, and thermal properties. The modular construction of the DBC scaffold, achieved through Cu(II)-catalyzed oxidative cyclization followed by cross-coupling functionalization, allows for easy access to a wide range of structurally diverse DBC derivatives. The resulting compounds exhibit strong emission with high PLQYs of up to 97% in solution, as well as excellent thermal stability, highlighting their potential as emissive materials for optoelectronic devices. Computational studies provided insight into their electronic structures, revealing that the degree of twisting between the DBC core and *N*-phenyl group influences the balance between locally excited states and CT character. Taken together, these results establish DBC derivatives as stable and tunable chromophores and provide design guidelines for their future applications in high-efficiency organic emitters and related photonic materials.

Author contributions

Minwoo Kong: conceptualization, data curation, formal analysis, investigation, methodology, visualization, writing – original draft. Ji Hye Lee: data curation, visualization. Heekyung Park: data curation, formal analysis, investigation. Hyonseok Hwang: data curation, visualization. Junseong Lee: data curation, formal analysis. Jun Hui Park: formal analysis, data curation, visualization. Myung Hwan Park: conceptualization, funding acquisition, supervision, visualization, writing – review and editing. Houng Kang: conceptualization, funding acquisition, supervision, visualization, writing – review and editing.

Conflicts of interest

There are no conflicts to declare.

Data availability

CCDC 2499642 contains the supplementary crystallographic data for this paper.[32]

All relevant data supporting the findings of this study are available within the article and its supplementary information (SI). Supplementary information: ^{1}H and ^{13}C NMR, crystallographic data, CV data, PL spectra, and computational data. See DOI: https://doi.org/10.1039/d5ra09166g.

Acknowledgements

This work was supported by the Academic Research Program of Chungbuk National University in 2024 and the Basic Science Research Program through the National Research Foundation, funded by the Ministry of Science and ICT of Korea (RS-2025-23523990 for M. H. Park and RS-2022-NR071826 for H. Kang).

References

1 B. Wex and B. R. Kaafarani, *J. Mater. Chem. C*, 2017, **5**, 8622–8653.
2 N. A. Kukhta, T. Matulaitis, D. Volyniuk, K. Ivaniuk, P. Turyk, P. Stakhira, J. V. Grazulevicius and A. P. Monkman, *J. Phys. Chem. Lett.*, 2017, **8**, 6199–6205.
3 P. Ledwon, *Org. Electron.*, 2019, **75**, 105422.
4 X. F. Luo, F. L. Li, J. W. Zou, Q. Zou, J. Su, M. X. Mao and Y. X. Zheng, *Adv. Opt. Mater.*, 2021, **9**, 2100784.
5 G. Sathiyan, E. K. T. Sivakumar, R. Ganesamoorthy, R. Thangamuthu and P. Sakthivel, *Tetrahedron Lett.*, 2016, **57**, 243–252.
6 L. G. Gao, T. H. Schloemer, F. Zhang, X. H. Chen, C. X. Xiao, K. Zhu and A. Sellinger, *ACS Appl. Energy Mater.*, 2020, **3**, 4492–4498.
7 M. Más-Montoya, J. P. Cerón-Carrasco, S. Hamao, R. Eguchi, Y. Kubozono, A. Tárraga and D. Curiel, *J. Mater. Chem. C*, 2017, **5**, 7020–7027.
8 C. H. Chen, Y. Wang, T. Michinobu, S. W. Chang, Y. C. Chiu, C. Y. Ke and G. S. Liou, *ACS Appl. Mater. Interfaces*, 2020, **12**, 6144–6150.
9 E. G. Cansu-Ergun and A. M. Önal, *J. Electroanal. Chem.*, 2018, **815**, 158–165.
10 Z. Xu, Y. L. Zhang, B. Z. Wang, Z. Liu, J. S. Zhao and Y. Xie, *Electrochim. Acta*, 2019, **302**, 373–384.
11 P. Gratia, A. Magomedov, T. Malinauskas, M. Daskeviciene, A. Abate, S. Ahmad, M. Grätzel, V. Getautis and M. K. Nazeeruddin, *Angew. Chem., Int. Ed.*, 2015, **54**, 11409–11413.
12 J. Ji, P. F. Li, Q. F. Tian, W. L. Feng and C. J. Wu, *Dyes Pigments*, 2019, **171**, 107670.
13 F. Liu, J. H. Zou, Q. Y. He, C. Tang, L. H. Xie, B. Peng, W. Wei, Y. Cao and W. Huang, *J. Polym. Sci., Polym. Chem.*, 2010, **48**, 4943–4949.
14 I. A. Pocock, A. M. Alotaibi, K. Jagdev, C. Prior, G. R. Burgess, L. Male and R. S. Grainger, *Chem. Commun.*, 2021, **57**, 7252–7255.
15 S. Oner and M. R. Bryce, *Mater. Chem. Front.*, 2023, **7**, 4304–4338.
16 C. Maeda, T. Todaka and T. Ema, *Org. Lett.*, 2015, **17**, 3090–3093.
17 V. V. Patil, K. H. Lee and J. Y. Lee, *J. Mater. Chem. C*, 2019, **7**, 14301–14305.
18 H. D. Xiang, W. Fan, J. H. Li, T. Y. Li, N. Robertson, X. R. Song, W. J. Wu, Z. H. Wang, W. H. Zhu and H. Tian, *Chemsuschem*, 2017, **10**, 938–945.
19 R. Braveenth, H. Lee, M. G. Song, K. Raagulan, Y. H. Park, S. Kim, J. H. Kwon and K. Y. Chai, *Dyes Pigments*, 2019, **163**, 607–614.
20 S. Vyskocil, M. Smrcina, M. Lorenc, I. Tislerová, R. D. Brooks, J. J. Kulagowski, V. Langer, L. J. Farrugia and P. Kocovsky, *J. Org. Chem.*, 2001, **66**, 1359–1365.
21 B. Y. Lim, M. K. Choi and C. G. Cho, *Tetrahedron Lett.*, 2011, **52**, 6015–6017.
22 C. K. Rank, A. W. Jones, T. Wall, P. Di Martino-Fumo, S. Schröck, M. Gerhards and F. W. Patureau, *Chem. Commun.*, 2019, **55**, 13749–13752.
23 M. Kong, A. Ghosh, M. H. Park, M. Kim and H. Kang, *Asian J. Org. Chem.*, 2025, **14**, e202400366.
24 P. J. Stephens, F. J. Devlin, C. F. Chabalowski and M. J. Frisch, *J. Phys. Chem.*, 1994, **98**, 11623–11627.
25 C. T. Lee, W. T. Yang and R. G. Parr, *Phys. Rev. B:Condens. Matter Mater. Phys.*, 1988, **37**, 785–789.
26 E. Runge and E. K. U. Gross, *Phys. Rev. Lett.*, 1984, **52**, 997–1000.
27 M. J. Frisch, G. W. Trucks, H. B. Schlegel, G. E. Scuseria, M. A. Robb, J. R. Cheeseman, G. Scalmani, V. Barone, G. A. Petersson, H. Nakatsuji, X. Li, M. Caricato, A. V. Marenich, J. Bloino, B. G. Janesko, R. Gomperts, B. Mennucci, H. P. Hratchian, J. V. Ortiz, A. F. Izmaylov, J. L. Sonnenberg, D. Williams-Young, F. Ding, F. Lipparini, F. Egidi, J. Goings, B. Peng, A. Petrone, T. Henderson, D. Ranasinghe, V. G. Zakrzewski, J. Gao, N. Rega, G. Zheng, W. Liang, M. Hada, M. Ehara, K. Toyota, R. Fukuda, J. Hasegawa, M. Ishida, T. Nakajima, Y. Honda, O. Kitao, H. Nakai, T. Vreven, K. Throssell, J. A. Montgomery Jr, J. E. Peralta, F. Ogliaro, M. J. Bearpark, J. J. Heyd, E. N. Brothers, K. N. Kudin, V. N. Staroverov, T. A. Keith, R. Kobayashi, J. Normand, K. Raghavachari, A. P. Rendell, J. C. Burant, S. S. Iyengar, J. Tomasi, M. Cossi, J. M. Millam, M. Klene, C. Adamo, R. Cammi, J. W. Ochterski, R. L. Martin, K. Morokuma, O. Farkas, J. B. Foresman and D. J. Fox, *Gaussian 6 Revision C.01*, Gaussian. Inc., Wallingford, 2016.
28 N. M. O'Boyle, A. L. Tenderholt and K. M. Langner, *J. Comput. Chem.*, 2008, **29**, 839–845.
29 R. P. Niu, Y. X. Wang, X. Z. Wu, S. Chen, X. R. Zhang and Y. L. Song, *J. Phys. Chem. C*, 2020, **124**, 5345–5352.
30 T. Nishiuchi, K. Kisaka and T. Kubo, *Angew. Chem., Int. Ed.*, 2021, **60**, 5400–5406.
31 S. Miertus, E. Scrocco and J. Tomasi, *Chem. Phys.*, 1981, **55**, 117–129.
32 CCDC 2499642: Experimental Crystal Structure Determination, 2026, DOI: 10.5517/ccdc.csd.cc2px2mb.